Latitude dependence of zonal plasma drifts obtained from dual-site airglow observations

C. Martinis,[1,2] J. V. Eccles,[3] J. Baumgardner,[1] J. Manzano,[4,5] and M. Mendillo[1]

Received 25 April 2002; revised 27 September 2002; accepted 19 December 2002; published 21 March 2003.

[1] All-sky imagers located at Tucumán, Argentina (26.9°S, 65°W, 14.2°S dip latitude), and Arequipa, Perú (16.5°S, 71.5°W, 2.7°S dip latitude), are used to track 630 nm airglow depletion motions in the first use of multisite airglow imagers for studies of low-latitude plasma dynamics. A new image analysis technique yields a consistent determination of nighttime zonal plasma drifts from all-sky images of the depletion motions. The observed eastward plasma drifts are smaller at Arequipa than at Tucumán in the postsunset period. During the postmidnight hours, the opposite pattern occurs. These observations are interpreted using the simple plasma drift model and coupled ionosphere-electric field model of *Eccles* [1998a, 1998b]. The observed zonal plasma drifts result from low-latitude electrodynamics with a mix of influences from *E* and *F* region conductivities and neutral wind shears in altitude and latitude. Analysis of the observations suggests that postsunset zonal drifts near the magnetic equator (Arequipa) are strongly influenced by the *E* region dynamo, while the *F* region dynamo is the main cause of zonal drifts observed closer to the Equatorial Ionization Anomaly (Tucumán). The observed altitude-latitude behavior of the plasma drifts gives the first two-dimensional evidence for the so-called *F* region plasma vortex's influence at equatorial and low latitudes obtained using optical imaging techniques. With this framework a synthesis is offered for seemingly inconsistent zonal drift observations in the published literature. *INDEX TERMS:* 2437 Ionosphere: Ionospheric dynamics; 2439 Ionosphere: Ionospheric irregularities; 2447 Ionosphere: Modeling and forecasting; 2415 Ionosphere: Equatorial ionosphere; *KEYWORDS:* ionosphere, all-sky imager, airglow observations, spread-F, plasma drifts, 630 nm

Citation: Martinis, C., J. V. Eccles, J. Baumgardner, J. Manzano, and M. Mendillo, Latitude dependence of zonal plasma drifts obtained from dual-site airglow observations, *J. Geophys. Res.*, *108*(A3), 1129, doi:10.1029/2002JA009462, 2003.

1. Introduction

1.1. Background

[2] Ionospheric plasma is free to flow along magnetic field lines according to ambipolar diffusion and neutral wind-forcing. Plasma drifts perpendicular to the magnetic fields are driven by electric fields in E × B motion. At low latitudes the perpendicular electric fields are created by neutral winds driving electric currents across magnetic field lines in a dynamo action in the E and *F* layers of the ionosphere [*Rishbeth*, 1971; *Heelis et al.*, 1974; *Kelley*, 1989]. At night, when the *E* region densities decay, the equations for the plasma motions can be greatly simplified using field-line integrated quantities and other nighttime assumptions [*Anderson and Mendillo*, 1983; *Haerendel et al.*, 1992; *Eccles*, 1998a]. These simple models show that a strong vertical polarization electric field is set up, which drives the plasma in the same direction and with nearly the same magnitude as the *F* region neutral wind.

[3] Observations of plasma drifts in the equatorial region have been widely studied using satellite and ground-based techniques. Using an extensive data set accumulated during 20 years of measurements with the incoherent scatter radar (ISR) at Jicamarca (12°S, 76.8°W, dip latitude 2°N), *Fejer* [1991] presented the seasonal, solar and magnetic dependence of the equatorial *F* region vertical and zonal plasma drifts. *Valladares et al.* [1996] presented results of the zonal drift of equatorial *F* region irregularities obtained by spaced-antenna satellite radio beacon (SRB) measurements of scintillation of 250 MHz signals from a geo-stationary satellite. These measurements were performed in 1994 at Ancón, Perú (11.8°S, 77.18°W, dip latitude 0.9°N). *Coley and Heelis* [1989] used horizontal and vertical ion drift data from the Dynamic Explorer 2 (DE-2) spacecraft to determine average zonal and vertical plasma flow in the ±26° dip latitude region during high solar activity. These equatorial and low-latitude studies showed that, under quiet magnetic conditions, nighttime zonal plasma drifts, dominated mainly by the *F* region dynamo, have been observed to be eastward, i.e., in the same direction as the *F* region neutral winds.

[1]Center for Space Physics, Boston University, Boston, Massachusetts, USA.
[2]Also at Departamento de Física, Universidad Nacional de Tucumán, Tucumán, Argentina.
[3]Space Environment Corporation, Logan, Utah, USA.
[4]Departamento de Física, Universidad Nacional de Tucumán, Tucumán, Argentina.
[5]Deceased September 1999.

0148-0227/03/2002JA009462$09.00

Table 1. Plasma Drift Studies From OI 630 nm Measurements in the South American Sector

		Optical Technique		Plasma Drifts		
Reference	Site[a]	All-Sky Imager	Scanning Photometer	Eastward	Westward	Magnetic Activity
Weber et al. [1978]	AIO	yes	no	yes	yes	moderate
Sobral and Abdu [1990]	CP	no	yes	yes	no	low
Sahai et al. [1994]	CP	no	yes	yes	no	low
Taylor et al. [1997]	AL	yes	no	yes	yes	moderate
Fagundes et al. [1997]	CP	yes	no	yes	no	low
Mendillo et al. [1997]	AR	yes	no	yes	no	low
Sobral and Abdu [1991]	CP	no	no	yes	no	low
De Paula et al. [2002]	CP	yes	no	yes	no	low

[a]AIO, Airborne Ionospheric Laboratory, West Coast of South America; CP, Cachoeira Paulista, 16°S dip latitude; AL, Alcantara, 0.3°S dip latitude; AR, Arequipa, 2.7°S dip latitude.

[4] There also have been observations on latitudinal variations of the nighttime plasma drifts, often with contradictory patterns reported. *Aggson et al.* [1987] deduced the eastward plasma flow from DE-2 satellite electric field measurements after sunset, when the satellite was near perigee at ~300 km; plasma drifts were larger in the off-equatorial region when compared with measurements in the equatorial region. The result was interpreted in terms of an altitude dependence of the *F* region dynamo electric field. *Coley and Heelis* [1989] showed a distinct peak at ~600 km in the equatorial vertical profile of the zonal plasma drifts in the sunset period. The peak was observed to move to lower altitudes (latitudes) as the night progressed, indicating that there was a local time dependence on its location. *Basu et al.* [1996] measured scintillation drifts for Ancón (dip 0.9°N) and Agua Verde (dip 11.0°S). These measurements indicated that the nighttime zonal drifts were smaller away from the magnetic equator between 22:00 and 23:00 LT. This latitude variation of the zonal drifts also was observed as a vertical shear of zonal drifts in radar maps at Jicamarca. Similarly, *Kil et al.* [2002], using Global Positioning System (GPS) scintillation measurements in Brazil during November–December, 1999, inferred the latitudinal variation of zonal plasma drifts between 20:00 and 02:00 LT. Their results showed higher eastward drift velocity at the magnetic equator in comparison to those near the peak of the Equatorial Ionization Anomaly (EIA).

[5] To interpret the results of plasma drifts observations, the proper determination of the vertical electric field at different local times is crucial in any attempted model. The vertical electric field in the equatorial region has been observed to vary strongly with altitude during the evening hours [*Valenzuela et al.*, 1980; *Tsunoda et al.*, 1981], causing a westward drift of plasma below the *F* peak and an eastward drift above. The vertical profiles of drift velocities calculated using Jicamarca radar data showed this shear [see *Kudeki et al.*, 1981; *Kudeki and Bhattacharyya*, 1999]. *Tsunoda et al.* [1981] showed that two dimensional plasma flow could be constructed at sunset by combining the zonal velocity and the vertical velocity components. The flow pattern resembled a vortex, with the velocity vector rotating clockwise when looking northward. *Haerendel et al.* [1992] modeled this vortex of flow with regions of westward and eastward flow during the early evening for equinoctial conditions. They determined that conductivity-weighted neutral wind dynamo, total conductance, and current divergence of the equatorial electrojet are three important inputs necessary for a complete formulation of the height variation of the vertical electric field.

[6] *Kudeki and Bhattacharyya* [1999] observations suggested that bottomside spread-F commences within the vortex, with the layer extending eastward into the nighttime ionosphere in the wake of the vortex. They pointed out that the properties of the vortex may have implications for the seeding or initiation of plasma bubbles that penetrate the *F* region.

1.2. Airglow Observations of Zonal Plasma Drifts

[7] Optical studies of plasma depletion motions were started when *Weber et al.* [1978] recorded the first 630 nm images of magnetically north-south aligned bands of depleted flux tubes, features shown to coincide with ionosonde measurements of equatorial spread-F (ESF). Many observations of these airglow depletions have been made since then [*Mendillo and Baumgardner*, 1982; *Mendillo et al.*, 1997; *Sahai et al.*, 1994; *Taylor et al.*, 1997; *Sinha and Raizada*, 2000]. The characteristics of these features establish that the depletions observed are the bottomside signatures of flux tube aligned plasma bubbles generated by the collisional gravitationally driven Rayleigh-Taylor plasma instability [*Kelley*, 1989].

[8] The key assumption made in the use of optical diagnostics to infer plasma drifts is that the zonal motion of airglow depletions can be considered equal to the ambient plasma flow. This is not true during the early explosive growth phase of an ESF plume. However, in well-developed depletions, the upward motion of the plasma has ceased or reduced, and the plume structure becomes strongly coupled to the zonal drifts. The motion of the airglow depletion boundaries should reflect zonal rather than vertical drifts in well-developed plumes.

[9] The motion of airglow depletions in OI 630 nm has been studied in the South-American sector using both scanning photometers and all-sky imagers. A summary of the main studies for this longitude sector appears in Table 1. It should be noted that the relatively small number of entries in Table 1 results from our restriction to reported dynamical effects. Many other references deal with occurrence statistics of airglow depletions or are studies showing general characteristics of the depletions.

[10] *Sobral and Abdu* [1990, 1991] used two 630 nm photometers to scan simultaneously (from the same site) in

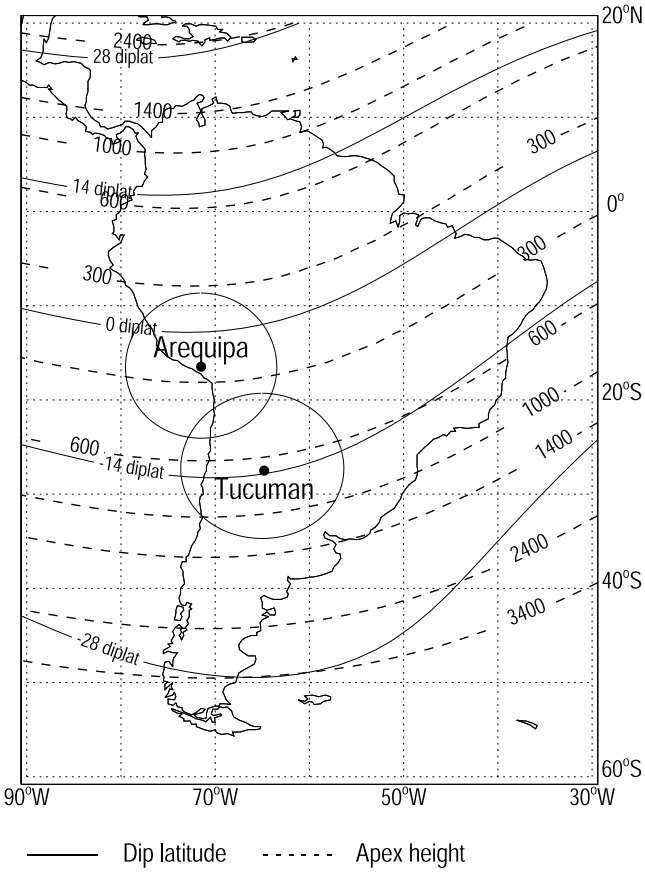

Figure 1. Map of South America showing the location of the all-sky imager sites. Circles represent the FOV of the instrument at an altitude of 250 km. Solid lines represent dip latitude; dashed lines represent apex height, defined as the peak altitude above the magnetic equator of a field line.

two east-west planes tilted 30° northward (apex height ~540 km) and 30° southward (apex height ~650 km) with respect to the zenith. Their measurements cover a time period of ~2 years, (1988–1990). A latitude gradient in the nighttime eastward drifts was detected, with the maximum speeds obtained in the northward (equatorial) scan direction. This gradient was attributed to a latitude gradient of the zonal neutral winds. All other entries in Table 1 describe drifts at zenith, and thus no latitude gradients were noted.

[11] In the Indian sector (80°E, dip 5.5°N), *Sinha and Raizada* [2000] obtained in 1993, from an all-sky imaging system, zonal plasma velocities that, early in the night, were slightly higher than those observed at Arequipa (dip 2.7°S) but smaller than those observed at Cachoeira Paulista (dip 16°S), suggesting the existence of a dip latitudinal dependence in the zonal velocities.

[12] The basic conclusion from 630 nm derived zonal drifts, at various latitudes and longitudes, is that the low-latitude region is dominated by eastward plasma drifts during the nighttime. Only a few cases showed occasionally westward drifts at midnight (see Table 1).

[13] In an attempt to address the zonal drift versus latitude issue in a consistent way, we present in this work the first coordinated set of low-latitude, ground-based plasma drift measurements in the same longitude sector using dual-site airglow-imaging techniques.

2. Observations and Analysis

2.1. Observations of Zonal Plasma Drifts

[14] We use identical all-sky CCD imaging systems in Arequipa, Perú, near the magnetic equator, and Tucumán, Argentina, closer to the peak of the EIA. Each system operates in a fully automated mode for fourteen days of each month, centered on the date of new Moon. Measurements are taken at several wavelengths, including OI 630 nm, the so-called oxygen red line. The vertical centroid of this emission is located at ~300 km early in the night (19:00–20:00LT) and later between 240 and 260 km [*Meriwether et al.*, 1997; *Martinis et al.*, 2001]. Both systems acquire images at alternating intervals of approximately 5 and 15 minutes. A complete description of such instruments can be found by *Baumgardner et al.* [1993], and a summary of the multiwavelength science topics capable of being studies at low latitudes appears in *Mendillo et al.* [1997].

[15] Figure 1 shows a map with the location of the sites. The circles represent the field of view of the instruments at a height of 250 km. Using a geomagnetic dipole field line model based on the international geomagnetic reference field (IGRF2000) in the Peruvian sector, apex heights (the peak altitude above the magnetic equator of a field line) and dip latitudes lines are also indicated. Because Arequipa is near the geomagnetic equator, the zenith airglow peak at 250 km above Arequipa is linked to the geomagnetic equator by nearly horizontal field lines at essentially the same height. At Tucumán, the airglow layer peak at 250 km represents the footprint of a flux tube that extends to ~650 km apex altitude.

[16] Airglow inferred plasma drifts can be obtained only on those nights when depletions occur, i.e., during ESF season for that site. At the longitudes of interest here, the ESF season corresponds to equinox [*Aarons*, 1993]. A pilot study was carried out for a three-year period that included both September/October and March/April periods. Data at both sites were taken during solar minimum conditions in equinox seasons during 1996 and 1997. A few additional nights in March 1998 were included in the Arequipa set. Unfavorable meteorological conditions over Tucumán during 1998 at the ESF season tended to eliminate most of the data from this site. Unfortunately, only one simultaneous night was available for the present analysis due to dissimilar cloud conditions at both sites. Nevertheless, average equinox trends at both sites should be reflected in the analysis below. Table 2 shows a summary of the data and geophysical conditions at the time of measurements.

[17] The following procedure was used to determine the velocities of the plasma depletions. Each image was projected onto a mercator map, assuming an airglow emission

Table 2. Summary of All-Sky Imager Data Used

	Arequipa Site	Tucumán Site
Number of days	26	17
Number of depletions	61	54
$\langle K_p \rangle$	2.3	2.1
$\langle F10.7 \rangle$	80	79

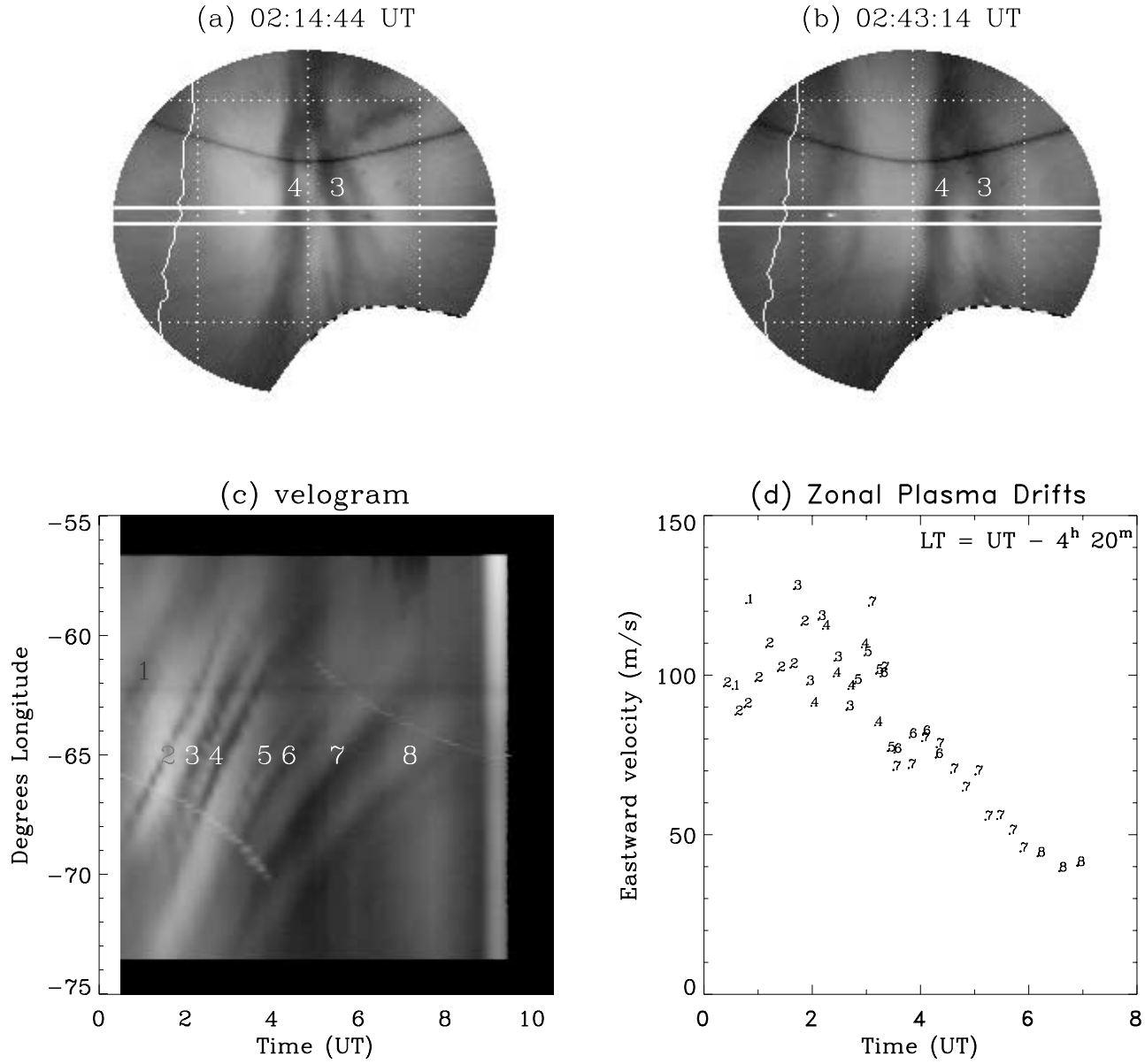

Figure 2. (a) and (b) show Tucumán images mapped to a 630 nm airglow layer mean height of 250 km at two different times on Oct. 26, 1997; (c) longitude vs. time diagram showing depletions that occurred this night; (d) plasma drifts inferred from panel c (see text).

height of 250 km. Figures 2a and 2b illustrate projected Tucumán images for October 26, 1997, with north at the top and east to the right of each image. The dark curved line at the top of the images is a defect on the image intensifier. The depletions marked 3 and 4 show the typical nighttime eastward motion. A 10-pixel wide, east-west slice, across the center of each image was averaged, and the resulting linear vector arrays were ordered in a two-dimensional array of longitude vs. time, a method of display termed a ''velogram'' (Figure 2c). The eastward motions of the depletions throughout the night appear as dark features progressing from the bottom left (west longitudes, early times) to the top right (east longitudes, later times). For each depletion we determined in the velogram the darkest x and y coordinates, with x representing time and y longitude. A combination of a Gaussian and second order polynomial was used to fit the cross section of the depletion at a given time. The average location of the darkest data value, the fitted curve's minimum value, and its centroid value was calculated. The velocity was then determined by taking the difference of every other average location value divided by their respective time difference. The average error in the determination of the velocity ranged from 5 to 20 m/s. Figure 2d shows the result for all the depletions observed during the night, with

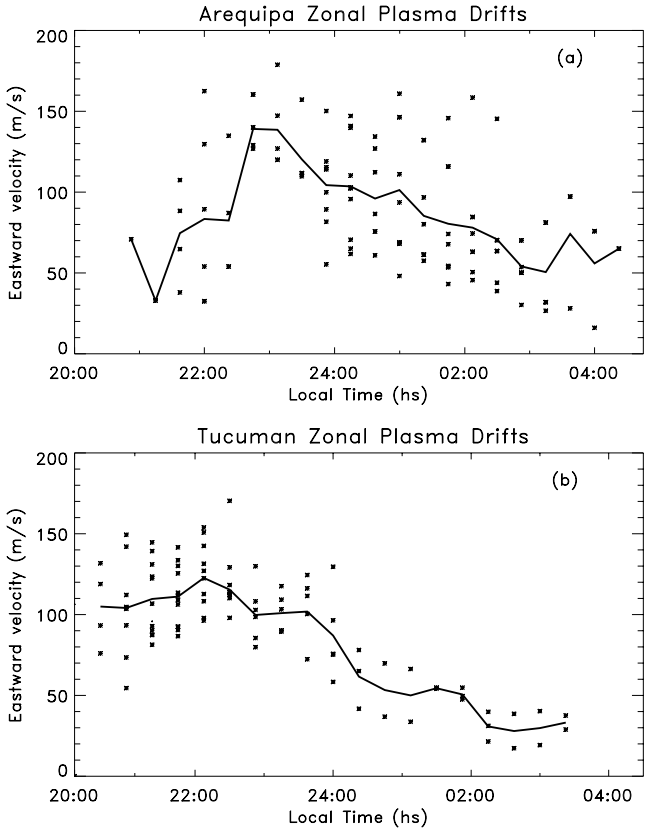

Figure 3. Zonal plasma drifts binned in 20-minute time intervals. (a) Arequipa, 26 nights. (b) Tucumán, 17 nights. Thick lines represent the average of each dataset.

each number representing a velocity point for the respective depletion. Figure 2 represents the first use of a fully automated technique for 630 nm derived plasma drift studies.

[18] Zonal plasma drifts from Arequipa and Tucumán determined with the method described above are shown in Figure 3. The final result is obtained by taking the average of 20-minute binned data for every night. Seventeen nights of Tucumán data were used, with a total of 54 depletions observed. Arequipa data consisted of 26 nights with 61 depletions. Arequipa drifts exhibit larger day-to-day variability, ranging from 20 m/s to 55 m/s, while Tucumán variability ranges from 15 m/s to 35 m/s.

[19] Figure 4a shows a smoothed version of each averaged curve in Figure 3, obtained by taking a three point running average smoothing. Arequipa's average peak velocity is ~130 m/s between 22:00–23:00 LT. Tucumán's average peak is ~120 m/s between 21:00–22:00 LT. Arequipa results are in general agreement with zonal plasma drifts from previous ground-based measurements at equatorial latitudes during solar minimum conditions [*Fejer*, 1991; *Valladares et al.*, 1996, 2002]. We thus feel confident in using the velogram technique at two sites to investigate latitude effects where comparisons of radio techniques are not available.

[20] In addition to the different local times of the maximum eastward drift note above, the Tucumán plasma drifts are larger than those at Arequipa early in the evening (before ~22:00–23:00 LT). After midnight, the situation is reversed and the plasma drifts at Arequipa are larger. These characteristic features observed in the entire data set are reproduced in the only common night of observations (October 26, 1997), as shown in Figure 4b.

2.2. Latitude Effects in Neutral Winds

[21] *Martinis et al.* [2001] compared Fabry-Perot Interferometer observations of thermospheric winds from two low-latitude sites at the same longitude of this study: Arequipa and Carmen Alto (dip 2.7°S vs. 10.2°S, respectively). A latitudinal dependence in zonal neutral winds was observed, i.e., winds at the equatorial site (Arequipa) were larger than at the off-equatorial site (Carmen Alto). Figure 5a shows a comparison of the neutral winds at Arequipa and Tucumán, the latter are calculated from the Carmen Alto winds using an empirical formula from *Anderson et al.* [1987]. Trying to match plasma velocities obtained from DE-2 satellite with theoretical profiles, *Anderson et al.* [1987] assumed a latitudinal dependence for the neutral winds proportional to cos (4ϕ), with ϕ representing the dip latitude. This relationship is consistent with the observed winds at Arequipa and Carmen Alto as shown in *Martinis et al.* [2001], even though it was originally used under solar

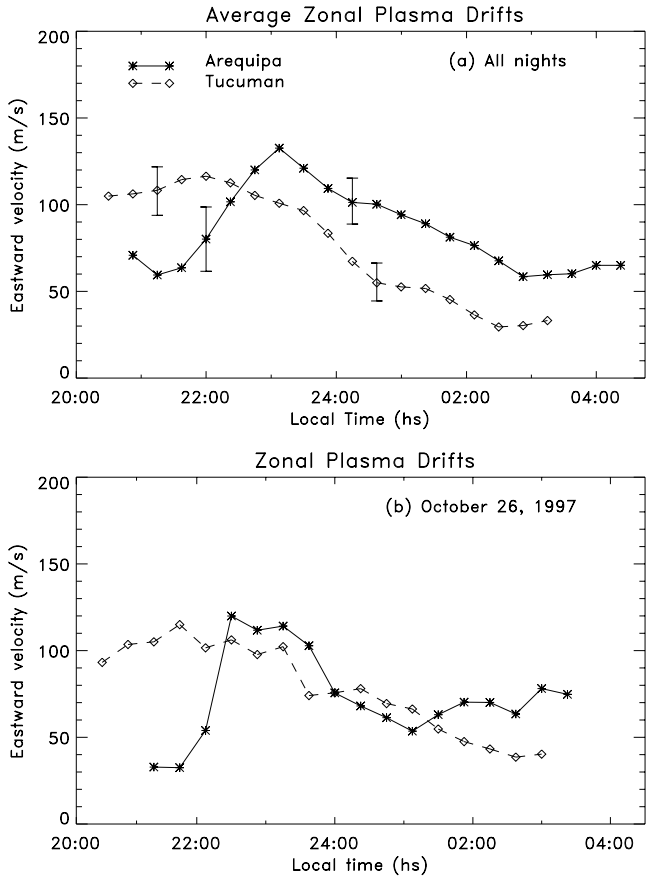

Figure 4. (a) Smoothed average zonal plasma drifts for total datasets at each site. Solid and dashed lines represent data from Arequipa and Tucumán, respectively. Vertical bars show errors of the mean; (b) Common night measurements on October 26, 1997, showing the same basic trend portrayed in panel a.

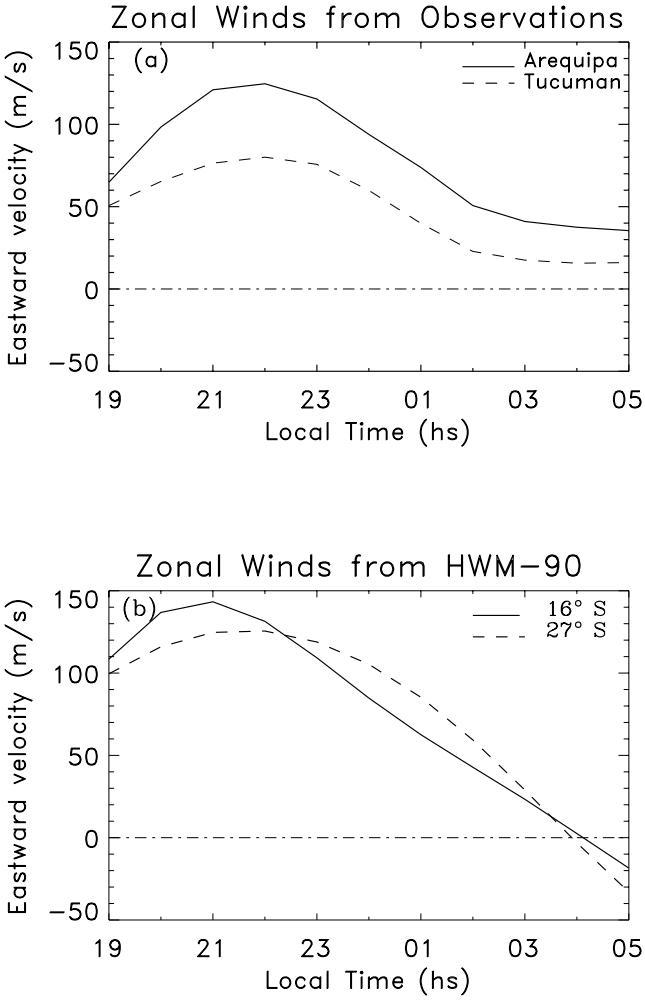

Figure 5. (a) Arequipa FPI's winds [from *Martinis et al.*, 2001], shown as solid lines. Tucumán winds, dashed lines, are calculated from an empirical formula using Carmen Alto FPI measurements (see text). (b) HWM-90 results at 250 km and 70°W. Solid lines represent output for 16°S, corresponding to the geographic latitude of Arequipa. Dashed lines show results for 27°S, geographic latitude of Tucumán.

maximum conditions at 23:00 LT. With no neutral winds measurements available for Tucumán, we used the empirical relationship to get $U_{Tuc} = 0.7\ U_{Car}$, where U_{Car} are the FPI winds measured at Carmen Alto.

[22] Recently, *Valladares et al.* [2002] showed that latitudinal gradients in neutral winds could be responsible for the effects observed in their comparisons of equatorial zonal winds and scintillations drifts. As discussed by *Martinis et al.* [2001], winds do indeed have a latitude dependence due to different ion-drag forces imposed by the latitude structure of the EIA. If the *F* region dynamo were to drive the plasma motion throughout the night, we would expect plasma drifts to follow the same latitudinal dependence of the winds, with Arequipa drifts larger than Tucumán drifts (dip 2.7°S vs. 14.2°S). We see such a relationship between the winds and the drifts only after 22:00–23:00 LT; that is, the difference of ~25–30 m/s in the winds at the two sites is approximately the same as in their plasma drifts. Figure 5b shows HWM-90 results at a longitude of 70°W for Arequipa and Tucumán latitudes. The pattern in this figure does not show a consistent difference between the two sites. The conclusion we draw from Figures 4 and 5a is that the plasma drifts can be explained by a simple *F* region dynamo arising from a latitudinal dependence of the neutral winds only after ~22:00–23:00 LT. Another mechanism is needed to explain the strong postsunset behavior, which shows larger drifts at Tucumán.

3. Plasma Drift Model and Results

3.1. Geometrical Considerations

[23] Zonal plasma drifts are driven by vertical electric fields. In the equatorial region, Pedersen conductivity is a crucial parameter in the determination of nighttime vertical electric fields. To illustrate the different contributions from *E* and *F* region Pedersen conductivities at each site, Figure 6 shows apex heights associated with the airglow layer above each site. The apex heights were calculated using dipole field geometry, an appropriate approximation for the small L-shell domain of equatorial aeronomy, which best fits the Peruvian magnetic meridian. Locations 'A' and 'B' represent typical "near-equatorial" and "near-EIA peak" latitudes, respectively. Flux tubes above 'B' penetrate the *F* region for all heights in the airglow layer (250–300 km). This is not the case for flux tubes above 'A'. At 250 km above 'A', most of the *F* layer is above the apex of the flux tube (~270 km). At a higher altitude above site 'A' (300 km), the corresponding field line does penetrate the *F* region and the *F* region conductivity component of the field-line-integrated conductivity increases. The relative contributions from *E* region and *F* region crossing components of a flux tube are clearly different for the two locations. After ~22:00 LT, vertical drifts reverse and the ionosphere drops, thereby increasing the *F* region contribution to the flux tube integrated conductivity above 'A' at both altitudes.

3.2. Model Description and Simulations

[24] Plasma drifts were calculated for average equinox conditions represented by Table 2 using the Ionospheric Forecast Model (IFM) [*Schunk et al.*, 1998] coupled with the electrodynamics model of *Eccles* [1998b]. The MSIS-1990 empirical atmosphere model [*Hedin*, 1991] provide the thermosphere densities. The *F* region winds are determined by the horizontal wind model (HWM-90) [*Hedin et al.*, 1991]. A simple tidal mode, used in previous low-latitude electrodynamics calculations [*Tarpley*, 1970; *Haerendel and Eccles*, 1992], replaced HWM winds at *E* region altitudes.

[25] The electrodynamics code is based on theory presented by *Haerendel et al.* [1992] and *Eccles* [1998b]. The electrodynamical model takes the local parameters from the ionosphere and thermosphere models and then calculates the flux tube integrated quantities of Pedersen conductivity (Σ_P) and Hall conductivity (Σ_H), Pedersen conductivity-weighted neutral wind (U_φ^P, U_L^P), and Hall conductivity-weighted neutral wind (U_φ^h, U_L^h). The coordinate system is a two-dimensional plane at the magnetic equator with *L* as the radial direction measured in earth radii and φ as the east-

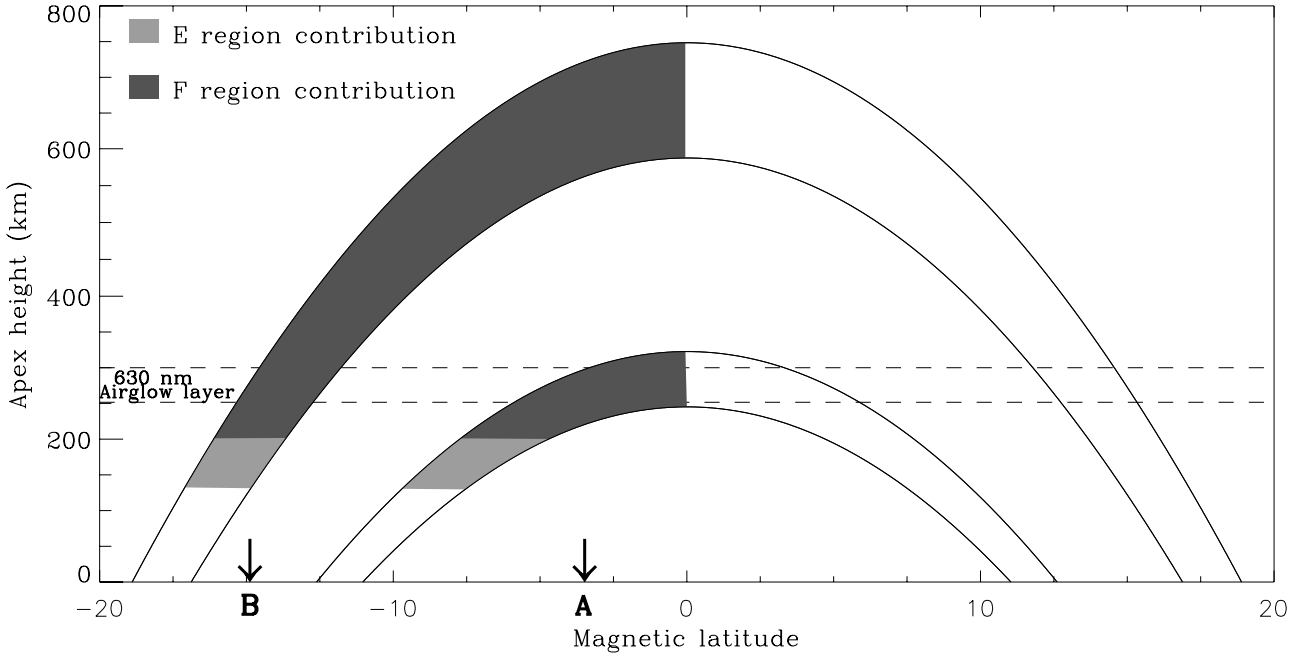

Figure 6. Illustration of geomagnetic dipole field geometry. Flux tubes over an equatorial station 'A' and a station 'B', near the Equatorial Ionization Anomaly, have different *E* and *F* region components. Light shadowing represents contributions of electron density and conductivity from *E* region portions of a flux tube, and dark shadowing represents *F* region contributions.

ward angle (longitude). The model solves the two-dimensional potential equation developed from the current continuity equation, which assumes equipotential field-lines [see *Eccles*, 1998a]. The solution to the potential equation yields plasma drifts in the magnetic dip-equator plane. Finally, the plasma drift velocities off the dip equator are determined through geometric considerations, assuming equipotential and dipolar field lines.

[26] Figure 7 shows the model plasma drift for the average conditions of the airglow measurements. The eve-

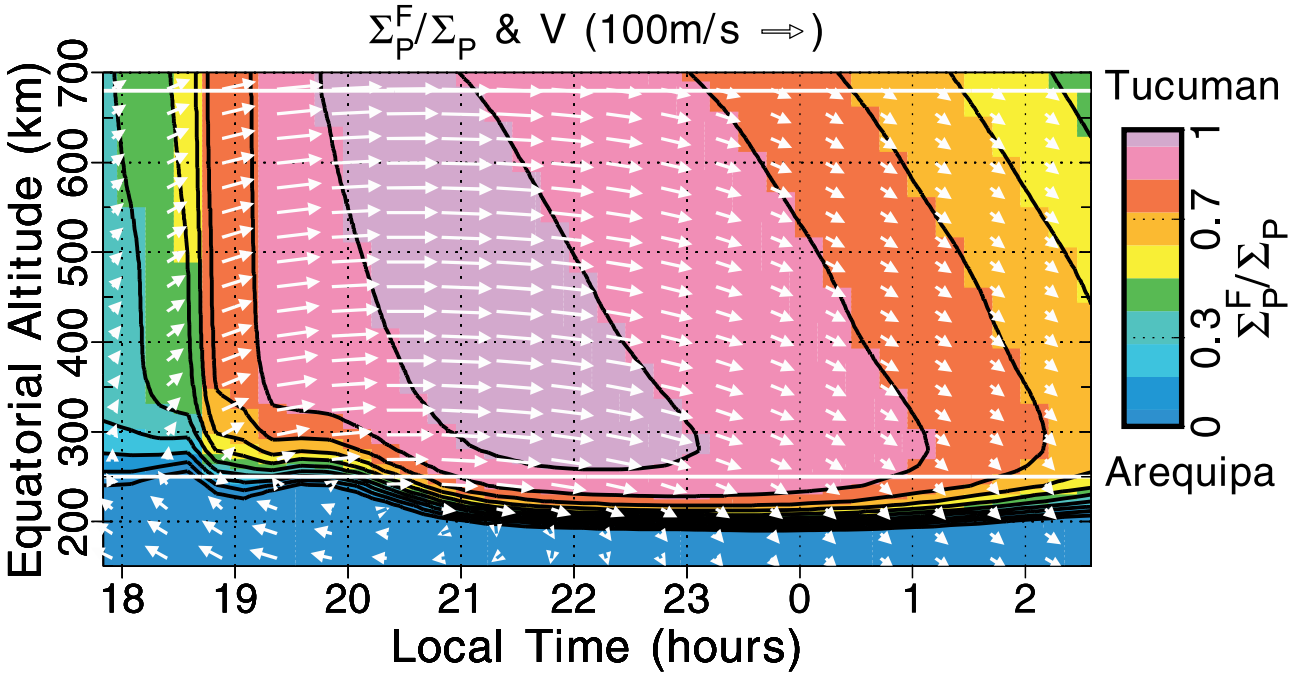

Figure 7. *F* region Pedersen conductivity to total Pedersen conductivity ratio as a function of local time on the magnetic equator plane. The vectors represent the plasma velocity field at the magnetic equator plane. Also shown the apex heights for Arequipa and Tucumán.

ning plasma drift vortex described in the introduction is evident in the plot. The focus of the vortex is at *E* region sunset (18:30LT) and in the *F* region bottomside. There is a clear closure of the vortex in the east (later times). Each site sees different plasma drifts at the different apex altitudes. The primary driver for the zonal plasma drifts is the zonal *F* region neutral wind, which drives meridional Pedersen currents. The bottom and top of the integrated *F* region (in conductivity) are the beginning and end of this dynamo current. A downward polarization electric field is set up to balance the dynamo current in the integrated *F* region. The downward electric field moves the plasma eastward with the neutral wind. There is an altitude variation in this vertical electric field. At lower apex altitudes, beneath the integrated *F* region, the *E* region winds dominate the creation of electric fields and cause a westward drift or smaller eastward drift. The *E* and *F* region dynamo effects can be examined using a simple formula relating the integrated conductivities and conductivity-weighted winds through the *E* and *F* region dynamos.

$$V_\varphi = U_\varphi^P - \frac{\Sigma_H}{\Sigma_P} V_L - \frac{J_L}{\Sigma_P} \quad (1)$$

$$U_\varphi^P = \frac{U_\varphi^{PF}\Sigma_P^F + U_\varphi^{PE}\Sigma_P^E}{\Sigma_P} \quad (2)$$

[27] The two-dimensional coordinate system at the plane of the dip equator is east longitude, φ, and altitude measured in earth radii, L. V_φ and V_L are the zonal and vertical plasma drifts, respectively. U_φ^P is the Pedersen-weighted neutral zonal wind. J_L is the integrated vertical current density. Σ_P and Σ_H are the total field-line integrated Pedersen and Hall conductivities. The *F* and E superscripts in equation (2) indicate partial flux tube integration through the *F* region only and through the two *E* regions [see *Haerendel et al.*, 1992]. Equation (1) is a one-dimensional solution for the zonal plasma drift. The zonal plasma drift is essentially equal to the total neutral wind dynamo, the first term, with remaining terms making adjustments below and above the peak of the integrated *F* region. The bottomside shear in the east-west drift defines the altitude where the *F* and *E* region dynamos (U_φ^{PF} and U_φ^{PE}) compete for domination (Equation 2). As stated above, airglow information from a "near-equatorial" site comes from the shear region near the *F* region bottomside. Slight changes in the height of the shear region will affect the results observed. Tucumán, on the other hand, has an airglow layer that maps to an apex height within or at the topside of the *F* region dynamo. The *E* to *F* region influence on the vertical electric field (or zonal drift) can be easily seen by comparing the ratio of the *F* region integrated conductivity to the total conductivity.

4. Discussion

[28] The airglow emission at OI 630 nm comes from a layer between 250 and 300 km. After ~20:00 LT, the centroid height of the airglow layer is found at ~250 km, remaining constant within ±10 km. In this height range, the model reproduces qualitatively the behavior of the plasma drifts at the two sites. There is, however, an important sensitivity to the magnetic field line's altitude above each site. The Arequipa airglow layer is located in the altitude

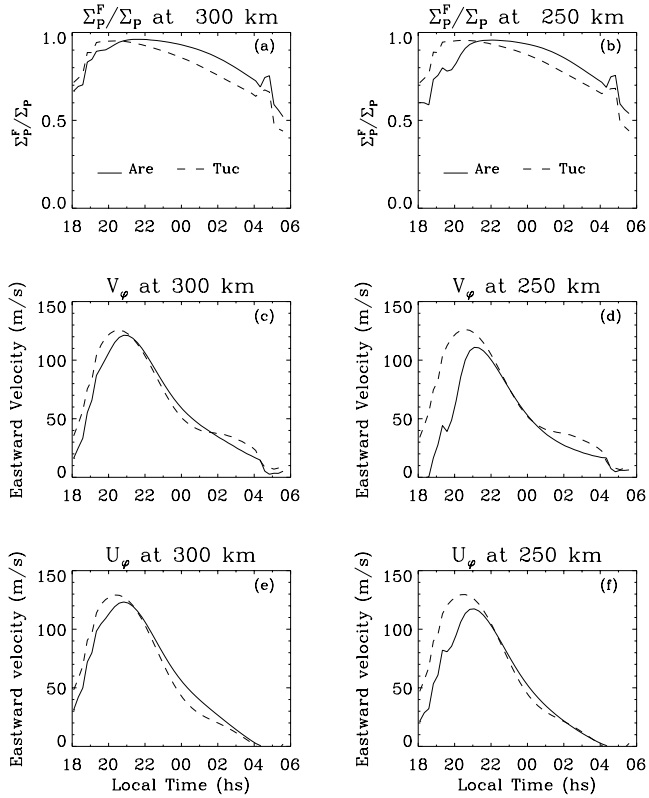

Figure 8. Model results for (a) *F* to total *E* and *F* regions conductivity ratio at 300 km and (b) at 250 km. (c) and (d): Model plasma drifts at 300 and 250 km, respectively. (e) and (f): Field-line integrated neutral winds above 300 and 250 km. Solid and dashed lines represent results for Arequipa and Tucumán, respectively.

region of the west-to-east shear drifts, described earlier, while Tucumán is located entirely in the eastward drift region. Arequipa's location in this shear region explains its lower plasma drifts relative to Tucumán before midnight as well as its larger day-to-day variability. The altitude of the shear in the zonal drift directly depends on the vertical drift at sunset [*Haerendel et al.*, 1992]. For the present conditions the model has very little vertical lift at sunset due to the low F10.7 value used. The shear region is found to be at ~250–280 km.

[29] The possible influence of upward motions affecting airglow-derived drifts would also be a concern if all of the airglow depletions come from evolving ESF bubbles. At Tucumán, all depletions observed are non-linear topside bubbles that drift zonally with the background plasma drift. The scatter in the Arequipa data, particularly in the early evening, is probably due to a mixture of early and late characteristics of the bottomside 'throat' of the bubbles. During the early development of plumes from the linear to non-linear stage, one might expect the airglow depletion not to be drifting with the background plasma flow, but suffering distortion along the edges of the dark band. Additionally, the altitude variation of the zonal drift at Arequipa can be large, adding to the possibility of variability in its airglow depletion drift.

[30] Figure 8a shows the ratio of *F* region to total field-line integrated Pedersen conductivities (Σ_P^F/Σ_P) for field

lines at 300 km above each site. After sunset, both ratios are large, meaning that the *F* region dynamo will be efficient in setting the plasma in motion. This is verified by looking at the model's plasma drifts at both sites in Figure 8c. For the overhead field lines at 250 km there are differences at the two sites. The postsunset conductivity ratio for Tucumán is still large, but the Arequipa ratio is somewhat smaller for the early evening hours (see Figure 8b). This means that *E* region effects will be important in the determination of the plasma drifts over Arequipa before ~22:00 LT, and, accordingly, the plasma drifts at Arequipa will be smaller than at Tucumán (Figure 8d). After ~22:00 LT, the ratios for both Arequipa and Tucumán are still large but decaying, and the plasma drifts above the two sites have similar values. At both altitudes, the model also shows that Arequipa drifts reach their maximum later (~1 hour) than the drifts above Tucumán.

[31] Figures 8e and 8f show the total integrated winds U_{φ}^{P} at 300 and 250 km. The field-line integrated HWM winds at both sites show differences in the postsunset period, especially at 250 km. Taken together, the different conductivity ratios (Figure 8b) and integrated HWM winds (Figure 8f) can explain the pattern of plasma drifts observed in the postsunset period (Figures 8d and 4).

[32] After ~22:00 LT the model does not reproduce the pattern observed. The differences may simply be due to the actual neutral winds behaving differently than those portrayed by HWM. A study of zonal plasma drifts is underway with HWM winds replaced by observed FPI wind patterns similar to those shown in Figure 5a.

[33] Our latitude patterns for plasma drifts provide a context in which to interpret seemingly inconsistent earlier observations. As pointed out by *Coley and Heelis* [1989], there is a local time dependence for the location of the maximum zonal drifts. Early in the night, the airglow measurements (showing larger off-equatorial (Tucumán) drifts) agree with the results from *Aggson et al.* [1987] and *Coley and Heelis* [1989]. But, later in the night, airglow measurements show larger equatorial (Arequipa) drifts, in agreement with the *Basu et al.* [1996] and *Kil et al.* [2002] observations. Yet, *Kil et al.* [2002] showed that prior to 22:00 LT the drifts at the equatorial site were higher, opposite to our observations and model. This could be explained by considering the different altitudes sampled by the optical and GPS scintillation measurements, which refer to irregularities from regions near 400 km. In the airglow layer, the postsunset contributions from *E* region conductivities are important at equatorial sites. However, at ~400 km, field line integrated quantities are dominated by *F* region effects (see Figure 6).

5. Conclusions

[34] In this work we presented results from the first coordinated airglow study of equatorial and low-latitude plasma drift measurements in the same longitude sector. The technique used to infer zonal plasma drifts from airglow depletion motions proved to be reliable: optically inferred zonal plasma drifts are in general agreement with past single-site measurements using radar and spaced-antenna scintillation techniques. However, coupled altitude-latitude effects determine specific patterns at a given site, and particularly so for the airglow layer.

[35] Our observational results show that, for quiet geomagnetic conditions, small eastward drifts occur early in the evening at latitudes where the *E* region dynamo is important. Accordingly, before midnight, Tucumán drifts are larger than those above Arequipa, while after midnight the opposite behavior is observed.

[36] The electrodynamics model [*Eccles*, 1998a, 1998b] used in this study provides the fundamental framework for understanding the differing plasma drifts observed at Tucumán and Arequipa. The plasma drifts above the two sites switch in relative strength at ~22:00 LT when the conductivity ratios cross over (Figures 8a and 8b). After ~22:00 LT both modeled drifts are very similar (Figures 8c and 8d), contrary to the observed drifts. It may be assumed that the less steep trend of the observed Arequipa plasma drifts compared to modeled Arequipa drifts results from a latitudinal variation in the neutral wind dynamos that is not well represented using the HWM zonal winds. The electrodynamics model uses flux tube integrated HWM winds that give similar values at Tucumán and at Arequipa, rather than the decreased values observed.

[37] When the levels of geomagnetic activity rise, westward drifts can be observed during the night (See Table 1). As discussed by *Taylor et al.* [1997], the reversal in the nighttime *F* region dynamo or the shift of the shear region to a higher altitude (placing the region of westward drifts in the airglow layer) could be responsible for the observed westward drifts. Thus, the ''mostly-east, but occasionally west'' patterns reported in the literature are understood as consistent with the coupled latitude vs. apex height patterns relating the 630 nm airglow layer to the low-latitude plasma vortex system. Additional observations of winds and drifts vs. latitude under quiet and disturbed conditions will further constrain coupled ionosphere-thermosphere-electrodynamics models and the horizontal wind model.

[38] **Acknowledgments.** This paper is dedicated to the memory of Professor José R. Manzano of the Universidad Nacional de Tucumán, Argentina, who initiated this airglow imaging aeronomy program in Argentina. We acknowledge the assistance and cooperation of Professors N. Ortiz de Adler and R. Ezquer. Also, C.M. acknowledges the support of Consejo Nacional de Investigaciones Cientificas y Tecnicas (CONICET). Funding support at Boston University was provided by the Office of Naval Research and the National Science Foundation Aeronomy Program. J. Wroten and T. Clark assisted in the data analysis. Funding support at Space Environment Corporation was provided by NSF Space Weather Program grant TM-9713418 and Air Force contract F19628-00-C0026.

[39] Arthur Richmond thanks Santimay Basu and H. Kil for their assistance in evaluating this paper.

References

Aarons, J., The longitudinal morphology of equatorial F-layer irregularities relevant to their occurrence, *Space Sci. Rev.*, *63*, 209–243, 1993.

Aggson, T. L., N. C. Maynard, F. H. Herrero, H. G. Mayr, L. H. Brace, and M. C. Liebrecht, Geomagnetic equatorial anomaly in zonal plasma flow, *J. Geophys. Res.*, *92*, 311–315, 1987.

Anderson, D. N., and M. Mendillo, Ionospheric conditions affecting the evolution of equatorial plasma depletions, *Geophys. Res. Lett.*, *10*, 541–544, 1983.

Anderson, D. N., R. A. Heelis, and J. P. McClure, Calculated nighttime eastward plasma drift velocities at low-latitudes and their solar cycle dependence, *Ann. Geophys.*, *5A*, 435–442, 1987.

Basu, S., et al., Scintillations, plasma drifts, and neutral winds in the equatorial ionosphere after sunset, *J. Geophys. Res.*, *101*, 26,795, 1996.

Baumgardner, J., B. Flynn, and M. Mendillo, Monochromatic imaging instrumentation for applications in aeronomy of the Earth and planets, *Opt.l Eng.*, *32*, 3028–3032, 1993.

Coley, W. R., and R. A. Heelis, Low-latitude zonal and vertical ion drifts seen by DE-2, *J. Geophys. Res.*, *94*, 6751, 1989.

De Paula, E. R., et al., Ionospheric irregularity zonal velocities over Cachoeira Paulista, *J. Atmos. Sol. Terr. Phys.*, *64*, 1511–1516, 2002.

Eccles, J. V., A simple model of low-latitude electric fields, *J. Geophys. Res.*, *103*, 26,699–26,708, 1998a.

Eccles, J. V., Modeling investigation of the evening prereversal enhancement of the zonal electric field in the equatorial ionosphere, *J. Geophys. Res.*, *103*, 26,709–26,719, 1998b.

Fagundes, P. R., Y. Sahai, I. Batista, J. Bittencourt, M. Abdu, and H. Takahashi, Vertical and zonal equatorial F-region plasma bubbles velocities determined from OI 630 nm nightglow imaging, *Adv. Space. Res.*, *20*, 1297–1300, 1997.

Fejer, B. G., Low-latitude electrodynamic plasma drifts: A review, *J. Atmos. Terr. Phys.*, *53*, 677–693, 1991.

Haerendel, G., and J. V. Eccles, The role of the equatorial electrojet in the evening ionosphere, *J. Geophys. Res.*, *97*, 1181–1197, 1992.

Haerendel, G., J. V. Eccles, and S. Çakir, Theory for modeling the equatorial evening ionosphere and the origin of the shear in the horizontal plasma flow, *J. Geophys. Res.*, *97*, 1209–1223, 1992.

Hedin, A. E., Extension of the MSIS thermospheric model into the middle and lower atmosphere, *J. Geophys. Res.*, *96*, 1159, 1991.

Hedin, A. E., et al., Revised global model of thermosphere winds using satellite and ground based observations, *J. Geophys. Res.*, *96*, 7657–7688, 1991.

Heelis, R. A., P. C. Kendall, R. J. Moffett, D. W. Windle, and H. Rishbeth, Electrical coupling of the E- and F-regions and its effects on F-region drifts and winds, *Planet. Space Sci.*, *22*, 743–756, 1974.

Kelley, M. C., *The Earth's Ionosphere*, Academic, San Diego, Calif., 1989.

Kil, H., P. M. Kitner, E. R. de Paula, and I. J. Cantor, Latitudinal variations of scintillation activity and zonal plasma drifts in South America, *Radio Sci.*, *37*, 1–7, 2002.

Kudeki, E., and S. Bhattacharyya, Post-sunset vortex in equatorial F-region plasma drifts and implications for bottomside spread-F, *J. Geophys. Res.*, *104*, 28,163–28,170, 1999.

Kudeki, E., B. J. Fejer, D. T. Farley, and H. M. Ierkic, Interferometer studies of equatorial F-region irregularities and drifts, *Geophys. Res. Lett.*, *8*, 377–380, 1981.

Martinis, C., J. Meriwether, M. Biondi, R. Niciewjewski, C. Fesen, and M. Mendillo, Zonal neutral winds at equatorial and low-latitudes, *J. Atmos. Sol. Terr. Phys.*, *63*, 1559–1569, 2001.

Mendillo, M., and J. Baumgardner, Airglow characteristics of equatorial plasma depletions, *J. Geophys. Res.*, *87*, 7641–7652, 1982.

Mendillo, M., J. Baumgardner, M. Colerico, and D. Nottingham, Imaging science contributions to equatorial aeronomy: Initial results from the MISETA program, *J. Atmos. Sol. Terr. Phys.*, *59*, 1587–1599, 1997.

Meriwether, J. W., M. A. Biondi, F. A. Herrero, C. G. Fesen, and D. C. Hallenback, Optical interferometric studies of the nighttime equatorial thermosphere: Enhanced temperature and zonal wind gradients, *J. Geophys. Res.*, *102*, 20,041–20,058, 1997.

Rishbeth, H., Polarization fields produced by winds in the equatorial F-region, *Planet. Space Sci.*, *19*, 357, 1971.

Sahai, Y., J. Aarons, M. Mendillo, J. Baumgardner, J. Bittencourt, and H. Takahashi, OI 630 nm imaging observations of equatorial plasma depletions at 16°S dip latitude, *J. Atmos. Sol. Terr. Phys.*, *56*, 1461–1475, 1994.

Schunk, R. J., J. J. Sojka, J. V. Eccles, and D. Thompson, Expanded capabilities for the ionospheric forecast model, *AFRL Rep. AFRL-VS-HA-TR-98-0001*, Air Force Res. Lab., Hanscom Air Force Base, Mass., 1998.

Sinha, H. S. S., and S. Raizada, Some new features of ionospheric plasma depletions over the Indian zone using all sky optical imaging, *Earth Planet. Space*, *52*, 549–559, 2000.

Sobral, J., and M. Abdu, Latitudinal gradient in the plasma bubble zonal velocities as observed by scanning 630 nm airglow measurements, *J. Geophys. Res.*, *95*, 8253–8257, 1990.

Sobral, J., and M. Abdu, Solar activity effects on equatorial plasma bubble zonal velocity and its latitude gradient as measured by airglow scanning photometers, *J. Atmos. Sol. Terr. Phys.*, *53*, 729–742, 1991.

Tarpley, J. D., The ionospheric wind dynamo, II, Solar tides, *Planet. Space Sci.*, *18*, 1091–1103, 1970.

Taylor, M. J., J. V. Eccles, J. LaBelle, and J. H. A. Sobral, High resolution OI (630 nm) image measurements of F-region depletion drifts during the Guará campaign, *Geophys. Res. Lett.*, *24*, 1699–1702, 1997.

Tsunoda, R. T., R. C. Livingston, and C. L. Rino, Evidence of a velocity shear in bulk plasma motion associated with the post-sunset rise of the equatorial F-layer, *J. Geophys. Res.*, *7*, 807–810, 1981.

Valenzuela, A., G. Haerendel, E. Fopl, H. Kappler, R. F. Woodman, B. Fejer, and M. Kelley, Barium cloud observations of shear flow in the postsunset equatorial F layer, *Eos Trans. AGU*, *61*, 315, 1980.

Valladares, C. E., R. Sheehan, S. Basu, H. Kuenzler, and J. Espinoza, The multi-instrumented studies of equatorial thermosphere aeronomy scintillation system: Climatology of zonal drifts, *J. Geophys. Res.*, *101*, 26,839–26,850, 1996.

Valladares, C. E., J. W. Meriwether, R. Sheehan, and M. A. Biondi, Correlative study of neutral winds and scintillation drifts measured near the magnetic equator, *J. Geophys. Res.*, *107*(A7), 1112, doi:10.1029/2001JA000042, 2002.

Weber, E. J., J. Buchau, R. H. Eather, and S. B. Mende, North-south aligned equatorial airglow depletions, *J. Geophys. Res.*, *83*, 712, 1978.

J. Baumgardner, C. Martinis, and M. Mendillo, Center for Space Physics, Boston University, 725 Commonwealth Ave., Boston, MA 02215, USA. (martinis@bu-ast.bu.edu)

J. V. Eccles, Space Environment Corporation, Logan, UT 84321, USA.